

D and B -meson production using k_t -factorization calculations in a variable-flavor-number scheme

B. Guiot^{*1} and A. van Hameren^{†2}

¹Departamento de Física, Universidad Técnica Federico Santa María;
Casilla 110-V, Valparaíso, Chile

²Institute of Nuclear Physics, Polish Academy of Sciences,
Radzikowskiego 152, 31-342 Kraków, Poland

Abstract

Within the framework of k_t -factorization, we compute the differential cross section for the production of B and D mesons, using a general-mass variable-flavor-number scheme. Our calculations include all relevant $2 \rightarrow 2$ processes. We explain how to include the $2 \rightarrow 1$ process in our calculations, but argue this is not (numerically) relevant at moderate transverse momentum. We apply this formalism to pp collisions and compare our results with ALICE and LHCb data at central and forward rapidity.

^{*}benjamin.guiot@usm.cl

[†]hameren@ifj.edu.pl

Contents

1	Introduction	2
2	Unintegrated PDFs: discussion on the scheme	3
3	The Watt-Martin-Ryskin unintegrated PDFs	5
4	The KaTie event generator	7
5	Comparison with data	8
5.1	<i>D</i> meson production	8
5.2	<i>B</i> meson production	12
5.3	<i>B</i> -meson production at very large rapidity	14
6	Treatment of the $2 \rightarrow 1$ process	15
7	Conclusion	17

1 Introduction

Heavy flavors, which play a particular role in perturbative Quantum Chromodynamics (pQCD), have been extensively studied. In the beginning, the observable was the total cross-section, plotted as a function of the center-of-mass energy \sqrt{s} . Later, with higher energies and statistics available, the differential cross-section has been measured, for instance, at the Tevatron and Large Hadron Collider (LHC). We note y as the rapidity of the detected heavy flavor and p_t as its transverse momentum. The theoretical description of this observable, requiring a more careful treatment compared to the total cross section, has known some troubles [1]. In the framework of collinear factorization, it is known that general-mass variable-flavor-number schemes (GM-VFNS) are more efficient than fixed-flavor-number schemes (FFNS) to describe the differential cross section at large p_t . By more efficient, we mean that, at a given order, the former gives better results than the latter, which is particularly true at leading order (LO). This better efficiency is partially explained by the fact that the GM-VFNS resums to all orders some large logarithms $\ln p_t^2/m_Q^2$, thanks to the heavy-quark distribution function.

Heavy-quark production has also been addressed by the first works on k_t factorization [2–5]. During the last two decades, heavy-flavor data have been compared to k_t factorization predictions by several groups, see for instance [6–11]. However, as pointed out in [12, 13], some of the available calculations are not performed consistently with respect to the choice of the scheme. One reason for this is simply the lack of appropriate unintegrated

parton distributions (uPDFs). Another reason is the complications coming from the use of off-shell matrix elements and the difficulty to compute the cross section at higher orders. The main goal of the present work is to provide for the first time kt -factorization calculations for D and B meson production, using a GM-VFNS.

In section 2, we have a general discussion on the schemes used in calculations. Then, we present our GM-VFNS uPDFs in section 3 and the event generator KaTie used for the evaluation of the off-shell cross section in section 4. In section 5, we compare our result to ALICE and LHCb data. Our calculations include all relevant $2 \rightarrow 2$ processes, which in k_t -factorization are next-to-leading order (NLO) contributions. In section 6, we discuss the implementation of the LO, $2 \rightarrow 1$, process and argue that it can be ignored at moderate transverse momentum, defined by $\alpha_s \ln p_t/m_Q \sim \mathcal{O}(1)$. Finally, we give our conclusion in section 7.

2 Unintegrated PDFs: discussion on the scheme

In collinear factorization, the cross section for heavy-quark production in hadron-hadron collisions is given schematically by

$$\sigma = \sum_{i,j} f_{i/h} \otimes f_{j/h} \otimes \hat{\sigma}(ij \rightarrow Q + X), \quad (1)$$

where $f_{k/h}$ is the collinear parton distribution for the parton k in the hadron h , and $\hat{\sigma}$ is the partonic cross section. Collinear PDFs are extracted by comparison of Eq. (1) with data. It is then clear that the output $f_{k/h}$ depends on the input $\hat{\sigma}$. A larger partonic cross section requires smaller PDFs, and the choice made for $\hat{\sigma}$ defines the scheme. Once the PDFs have been extracted, they can be used to make predictions. However, the new partonic cross section should be computed with the scheme used in the extraction of the PDFs.

The situation is similar in k_t factorization. The cross section reads

$$\begin{aligned} \frac{d\sigma}{dx_1 dx_1 d^2 p_t}(s, x_1, x_2, p_t^2) &= \sum_{i,j} \int_0^{k_{t,\max}^2} d^2 k_{1t} d^2 k_{2t} F_{i/h}(x_1, k_{1t}^2; \mu^2) \\ &\times F_{j/h}(x_2, k_{2t}^2; \mu^2) \hat{\sigma}(x_1 x_2 s, k_{1t}^2, k_{2t}^2, p_t^2; \mu^2), \end{aligned} \quad (2)$$

where the uPDFs, $F_{k/h}(x, k_t^2; \mu^2)$, depend on x , the fraction of the hadron longitudinal momentum carried by the parton, k_t , the initial parton transverse momentum, and μ , the factorization scale. $\hat{\sigma}$ is the off-shell cross section. The uPDFs are generally not extracted from data¹, but built from

¹An exception is the PB uPDFs [14]

the collinear PDFs by inverting the relation:

$$f_{k/h}(x, \mu^2) = \int^{\mu^2} F_{k/h}(x, k_t^2; \mu^2) d^2 k_t. \quad (3)$$

Note that different versions of this relation can be found in the literature. It is clear that the scheme of the uPDFs built from Eq. (3) should be identified to the scheme of the collinear PDFs appearing in this equation. Everything we said on the scheme is also true for the order of calculation. As a consequence, the different sets of uPDFs available on the TMDlib [15, 16] cannot be compared by simply using them with the same cross section, as they have been obtained in different schemes and at different orders. For our present study, we will use uPDFs and off-shell cross sections obtained in a GM-VFNS at order $\mathcal{O}(\alpha_s^2)$.

The numerical consequence of using a cross section at an order/scheme different from that of uPDFs depends on the case. Mixing the VFNS and FFNS could lead to the wrong estimation of the cross section for charm production by a factor of 4 [12, 13]. Indeed in the VFNS, the cross section obtained at order $\mathcal{O}(\alpha_s^2)$ reads

$$\sigma(\text{charm}) = \sum_{i,j} f_i^{\text{VFNS}, (2)} \otimes f_j^{\text{VFNS}, (2)} \otimes \hat{\sigma}^{(2)}(\text{FEP} + \text{FCP}), \quad (4)$$

where FEP stands for flavor excitation processes, e.g. $cg \rightarrow cg$, and FCP for flavor creation processes, e.g. $gg \rightarrow c\bar{c}$.² On the opposite, using the FFNS, we have

$$\sigma(\text{charm}) = \sum_{k,l} f_k^{\text{FFNS}, (2)} \otimes f_l^{\text{FFNS}, (2)} \otimes \hat{\sigma}^{(2)}(\text{FCP}). \quad (5)$$

We changed the subscript to k and l to point out that the sums in Eqs. (4) and (5) are not identical. We know that $\hat{\sigma}^{(2)}(\text{FEP} + \text{FCP}) \sim 4\hat{\sigma}^{(2)}(\text{FCP})$, due to the large contribution of the flavor excitation process $cg \rightarrow cg$. Then, we deduce that

$$\sum_{i,j} f_i^{\text{VFNS}, (2)} \otimes f_j^{\text{VFNS}, (2)} \sim \frac{1}{4} \sum_{k,l} f_k^{\text{FFNS}, (2)} \otimes f_l^{\text{FFNS}, (2)} \quad (6)$$

Consequently, using the VFNS PDFs with $\hat{\sigma}(\text{FCP})$ implies an underestimation of the cross section by a factor of 4. The (numerical) situation could improve at higher orders if $\hat{\sigma}(\text{FCP})$ and $\hat{\sigma}(\text{FEP} + \text{FCP})$ are numerically closer, but mixing different schemes is always inconsistent and dangerous.

²The number two in parenthesis indicates that we work at the order $\mathcal{O}(\alpha_s^2)$.

Strictly speaking, calculations performed in [12] are not completely consistent since the NLO PB uPDFs [14], being, in fact, next-to-next-to-leading order (NNLO) in k_t -factorization, have been combined with a NLO cross section ($\mathcal{O}(\alpha_s^2)$). However, the numerical deviation from the calculations performed in the present paper is found to be small. The interest of the present work is to provide consistent GM-VFNS k_t -factorization calculations.

3 The Watt-Martin-Ryskin unintegrated PDFs

Accordingly to Eq. (3), VFNS uPDFs of order $\mathcal{O}(\alpha_s^2)$ can be built from collinear PDF extracted in this scheme and at this order. In the WMR approach [17], the uPDF for a parton a reads

$$F_a(x, k_t^2; \mu^2) = \frac{1}{k_t^2} T_a(\mu, k_t) \sum_{a'} \int_x^{1-\Delta} \frac{dz}{z} \frac{\alpha_s(k_t)}{2\pi} P_{aa'}(z) f_{a'}\left(\frac{x}{z}, k_t\right). \quad (7)$$

where $P_{aa'}(z)$ are the usual unregulated splitting functions, except for P_{gg} given by

$$P_{gg} = 2C_A \left[\frac{z}{1-z} + \frac{1-z}{z} + z(1-z) \right], \quad (8)$$

and $T_a(\mu, k_t)$ is the Sudakov factor defined by

$$T_a(\mu, k_t) = \exp \left\{ - \int_{k_t^2}^{\mu^2} \frac{dp_t^2}{p_t^2} \sum_{a'} \int_0^{1-\Delta(p_t)} dz z \frac{\alpha_s(p_t)}{2\pi} P_{a'a}(z) \right\}. \quad (9)$$

A possible choice for Δ is the strong ordering cut-off

$$\Delta(q) = \frac{q}{\mu}, \quad (10)$$

with $\mu \sim \sqrt{p_t^2 + m^2}$ the factorization scale. With this cut-off,

$$F_a(x, k_t^2; \mu^2) = 0 \quad \text{if } k_t > \mu. \quad (11)$$

However, the strong ordering cut-off does not stem from fundamental considerations, and the obtained uPDFs do not fulfill relation (3) with good precision. This is due to the fact that Δ is too large and cuts half of the integral when $k_t = 0.5\mu$. Consequently, we keep the condition (11) and use Δ/d , with $d > 1$ chosen such that the relation (3) is satisfied.

We built our uPDFs using the WMR formalism and the leading order CT14 PDFs [18]. These collinear PDFs have been extracted using the ACOT $_{\chi}$ scheme [19–21]. Our uPDFs are shown in figures 1 and 2, where we plot eq. (3) as a function of μ^2 for different values of x . We observe a global good agreement, in particular at small x .

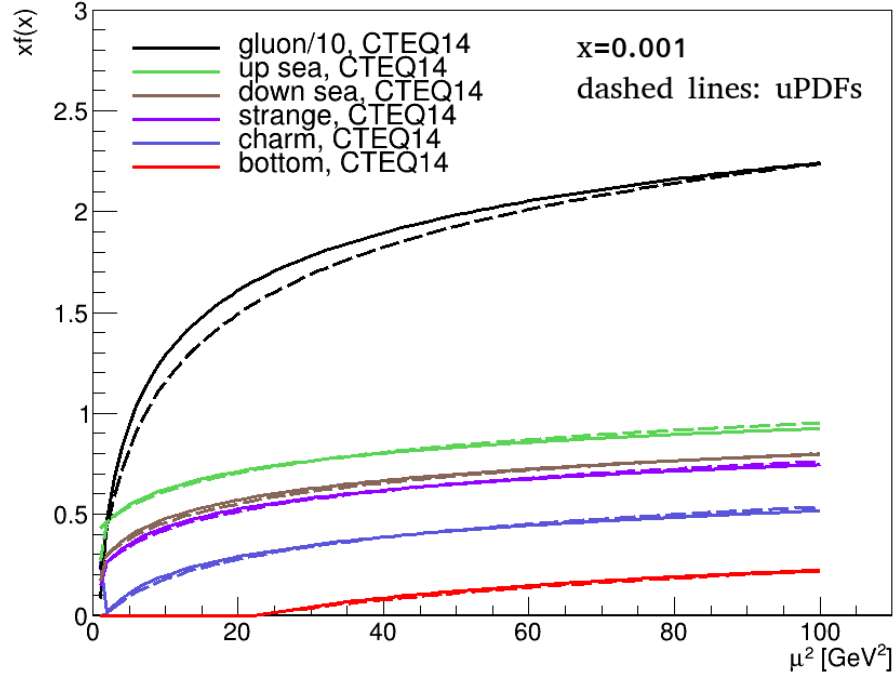


Figure 1: Comparison of CT14 LO parton distributions (full lines) at $x = 0.001$ with the integrated uPDFs (dashed lines), see eq. (3).

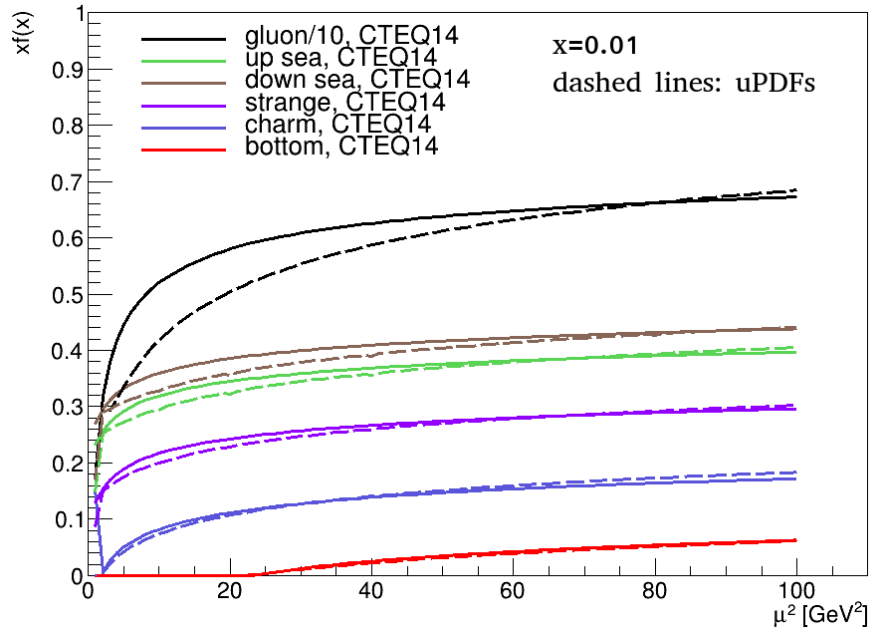


Figure 2: Same as Fig. 1 for $x = 0.01$.

4 The KaTie event generator

The calculations in the following have been performed with the help of the parton-level event generator KaTie [22]. It can generate events for which the partonic initial-state momenta are space-like and have non-vanishing transverse components. The necessary uPDFs can be provided by TMDlib or as grid files in text format. In the latter case, KaTie takes care of the interpolation. KaTie operates at tree level and can deal with any processes within the standard model. It generates events employing importance sampling and numerically evaluates the matrix element using helicity amplitudes. The events are stored in event files which can be chosen to be in the LHEF format [23]. It is, however, also possible to make histograms directly using the provided tools.

The initial-state and final-state momenta are generated satisfying exact kinematics. Within k_t factorization, this means that the initial-state momenta $k_i^\mu = x_i P_i^\mu + k_{it}^\mu$ are space-like, with a longitudinal component along the light-like momentum P_i^μ of either colliding hadron, plus transverse components k_{it}^μ . The matrix elements are constructed as described in [24, 25], as summed squares of helicity amplitudes. The essence of the method is that a space-like external parton is represented as a pair of auxiliary light-like partons satisfying eikonal Feynman rules, leading to manifestly gauge invariant amplitudes with exact kinematics.

In this paper, we consider parton-level processes that, within collinear factorization, would involve massive initial-state quarks with time-like momenta. The same construction of the amplitudes with space-like initial-state momenta leads also for these processes to manifestly gauge invariant matrix elements. The only restriction is that the transverse momentum of the initial-state parton must not be much smaller than the mass. While gauge invariance is guaranteed, the correct on-shell limit cannot be reached for time-like momenta by naively taking very small transverse momentum. Note that the kinematics of the final-state massive quark is always exact, with its momentum time-like $p^2 = m_Q^2$.

As mentioned earlier, KaTie operates at tree level. The tree-level matrix elements contain singularities as functions of the external momenta when these become soft or collinear with each other. In particular, the matrix elements behave singularly if a final-state gluon momentum becomes collinear with the momentum of an initial-state hadron. The latter also happens in k_t factorization. We will consider partonic processes with a final-state gluon, which suffer from such a collinear singularity. In usual tree-level calculations, these singularities are avoided by phase space cuts that define the jet observables, for example, the demand of a minimal transverse momentum. We also use a small minimum on the transverse momentum to avoid the singularity. We see that the cross section depends only very mildly on this phase space cut if we vary the minimum between 0.5 GeV and 2.0 GeV, the

latter being of the order of the mass of the quarks we are considering.

5 Comparison with data

5.1 D meson production

Working with a GM-VFN scheme, the following processes are included

$$gg \rightarrow Q\bar{Q} \quad q\bar{q} \rightarrow Q\bar{Q} \quad (12)$$

$$gQ \rightarrow gQ \quad qQ \rightarrow qQ \quad \bar{q}Q \rightarrow \bar{q}Q, \quad (13)$$

where Q represents the heavy quark and q a light quark. The first and second lines correspond to flavor-creation and flavor excitation processes, respectively. For consistency, we choose the charm mass equal to the one used for the CT14 PDFs, e.g., $m_c = 1.3$ GeV. For the fragmentation of a charm quark into a D meson, we use the Peterson model of fragmentation function [26] with $\epsilon_c = 0.05$, and the fragmentation fractions given in table 1. The three first values are those used by FONLL [27].

$f(c \rightarrow D^0)$	$f(c \rightarrow D^+)$	$f(c \rightarrow D^{*+})$	$f(c \rightarrow D_s^+)$
0.588	0.234	0.234	0.116

Table 1: Charm to D -meson fragmentation fractions.

The result for the p_t distribution of D^0 mesons is compared to ALICE data [28] in figure 3. The error band corresponds to the factorization scale uncertainty, evaluated as usual by the variation of a factor of $\sqrt{2}$ above and below the central value, chosen to be

$$\mu = \frac{1}{2}(m_{t,1} + m_{t,2}), \quad (14)$$

where $m_{t,i} = \sqrt{p_{t,i}^2 + m_c^2}$. The subscripts 1, 2 label outgoing partons. One of these partons is a charm, since processes such as $gg \rightarrow gg$ with a final gluon fragmenting into a D meson are negligible and have not been considered. Note that we use $m_{t,i}$ even if $p_{t,i}$ corresponds to a gluon or light quark transverse momentum. In collinear factorization, the usual choice for the factorization scale is

$$\mu = m_t, \quad (15)$$

with m_t the charm transverse mass. In the limit where the transverse momentum of the initial partons goes to zero, $k_{1t}, k_{2t} \rightarrow 0$, Eqs. (14) and (15) coincide. In figure 4, we compare our calculations for the p_t distribution of D^+ mesons with ALICE data. We observe a good agreement on the full p_t range, and the central value alone provides a good description, except

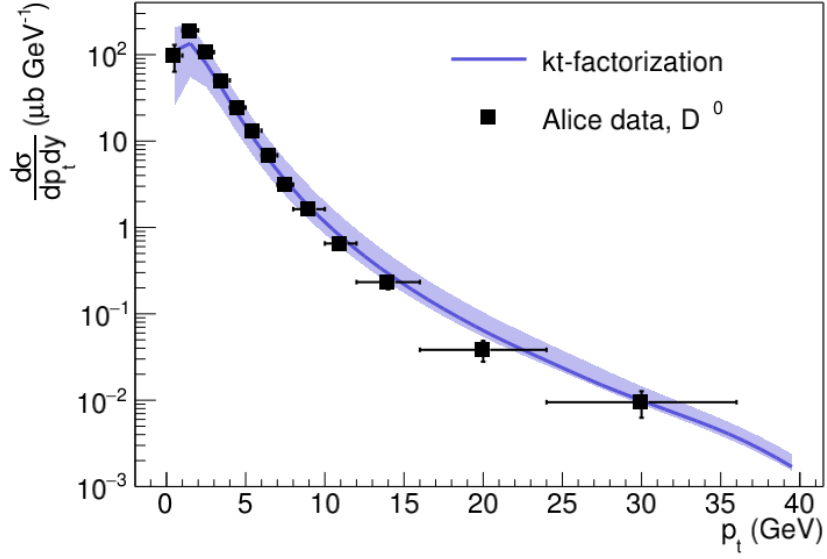


Figure 3: Leading order k_t -factorization calculations, obtained in a GM-VFNS, compared to ALICE data [28] for D^0 mesons. The line shows the central value of our calculations and the band corresponds to the factorization scale uncertainty.

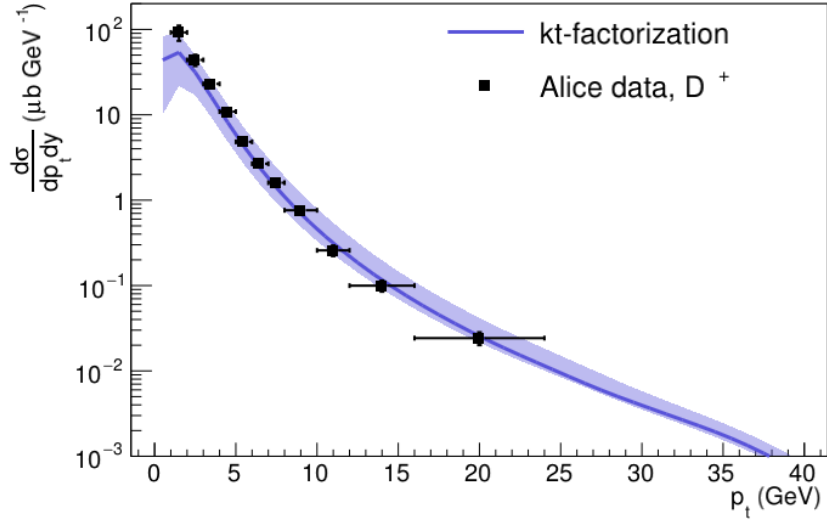


Figure 4: Same as Fig. 3 for D^+ mesons.

for the first bin of Fig. 4. A Comparison with figure 5 of Ref. [28] shows that the underestimation of D -meson data at small transverse momentum by theoretical calculations is usual. We will see in the next section that this is not the case for B mesons. Compared to the k_t -factorization calcu-

lations available in the literature, the description of D mesons' transverse momentum has been improved³. We believe this is directly related to the consistent use of a GM-VFNS. To reach a similar result in an FFNS, it is probably necessary to include higher orders. Similar results obtained at 7 TeV for D^{*+} and D_s^+ are presented at the end of this paper in Fig. 13. We turn now our attention to ALICE measurement at 5 TeV [29]. The data, not yet available on HEPData, are presented without error bars, see Fig. 5. Within uncertainties, the agreement with our calculations is excellent.

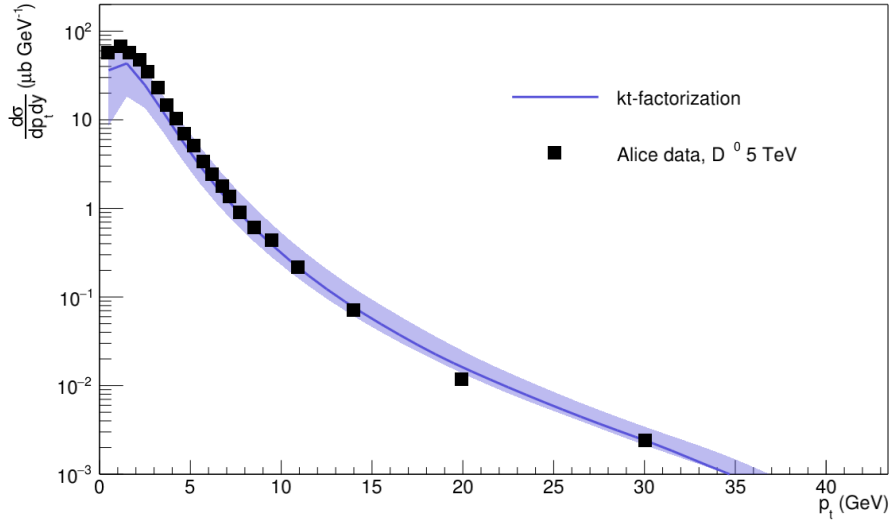


Figure 5: D^0 production at 5 TeV compared with ALICE data [29].

We can also explore the production of D mesons at larger rapidities and energies. In Fig. 6, we compare our calculations with LHCb data [30] at 13 TeV in the rapidity range $2 < y < 2.5$. Using the same set of parameters, we obtained a description of experimental data of similar quality compared to the central rapidity case. What has changed is the relative contributions of flavor excitation and creation processes. Indeed, in figure 7, we observe that at forward rapidity the two contributions are closer (green and red curves). The interplay between flavor-excitation and flavor-creation processes being absent in an FFNS at order $\mathcal{O}(\alpha_s^2)$ is probably another good reason for using a GM-VFNS.

Finally, we quickly discuss other theoretical uncertainties related to our calculations. In Fig. 8 we show the result of varying the charm mass from 1.3 to 1.5 GeV. We observe only a small effect at small transverse momen-

³It can be seen, for instance, by comparing our results with the predictions in green of Ref. [28].

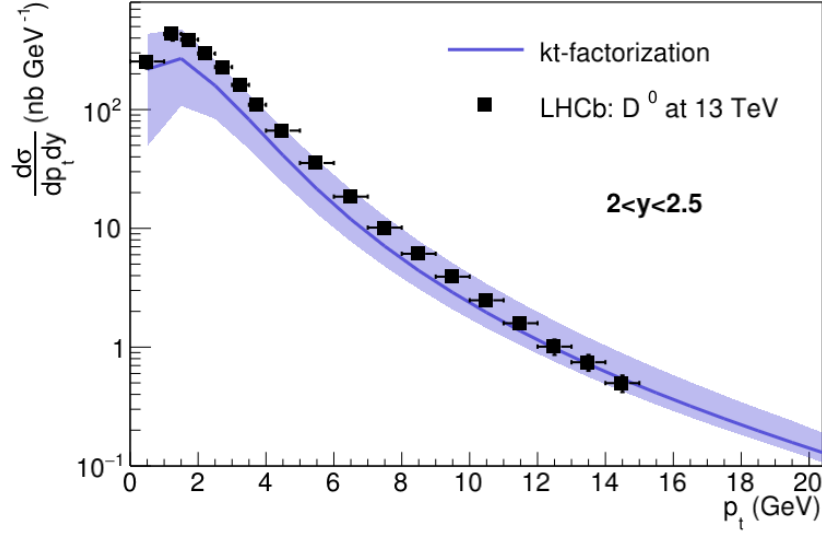


Figure 6: D^0 production at 13 TeV compared with LHCb data [30] in the rapidity range $2 < y < 2.5$.

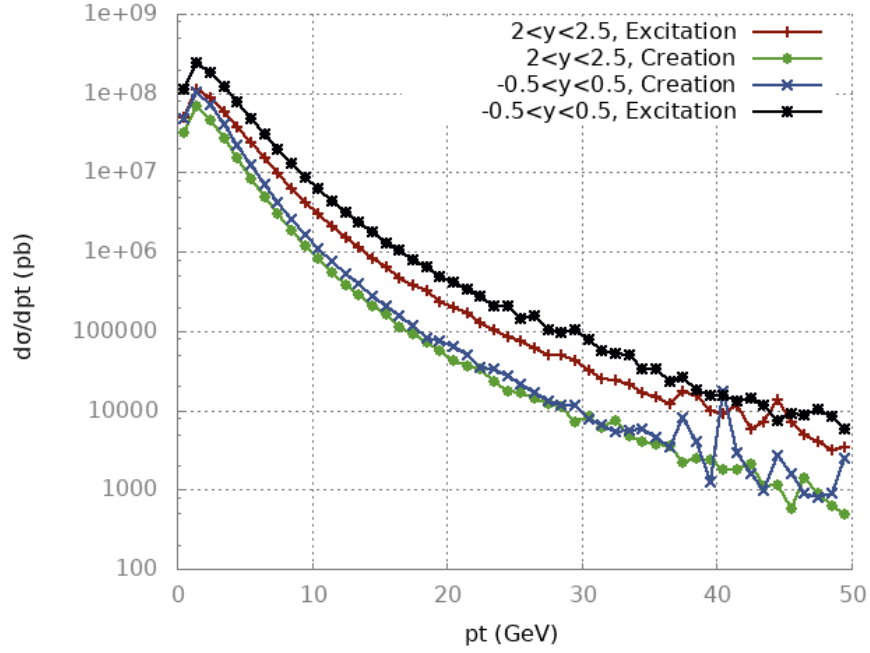


Figure 7: Comparison of flavor-excitation and flavor-creation cross sections at central rapidity (7 TeV) and forward rapidity (13 TeV). The green and red curves are closer than the blue and black curves

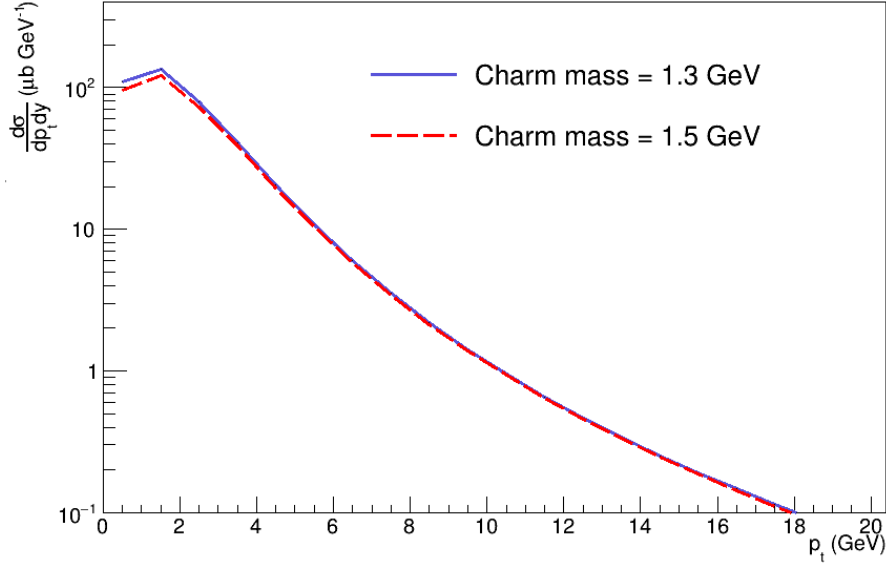


Figure 8: D^0 transverse momentum distribution for two different charm masses.

tum. Similarly, varying the p_t cuts described in section 4 by a factor of 2 has only a small impact. The uncertainty related to the choice for the fragmentation function has been studied in [9]. Note that we use the same fragmentation function with the same value of the parameter ϵ_c .

5.2 B meson production

Changing Q by b in (12) and (13) gives the complete list of the processes considered. In particular, we did not take into account the $cb \rightarrow cb$ process. In agreement with the CT14 PDFs, the bottom mass is set to $m_b = 4.75$ GeV. We use the Perterson fragmentation function with $\epsilon_b = 0.01$ and the factorization scale Eq. (14) with $m_{t,i} = \sqrt{p_{t,i}^2 + m_b^2}$. In agreement with the discussion in [31], we choose the fragmentation fraction $f(b \rightarrow B^+) = f(b \rightarrow B^0) = 0.403$.

The LHCb collaboration measured the B^\pm double-differential cross sections at 7 TeV and 13 TeV, in the rapidity range $2 < y < 4.5$ [32]. In Fig. 9, we compare our results to LHCb data at 7 TeV and $2 < y < 2.5$. We observe a global good agreement with our central predictions, with a slight overestimation at $p_t \sim 5$ GeV. All experimental data lay within theoretical uncertainties, estimated by varying the factorization scale. The uncertainty band is broader than for D mesons, which is due to the dependence of the

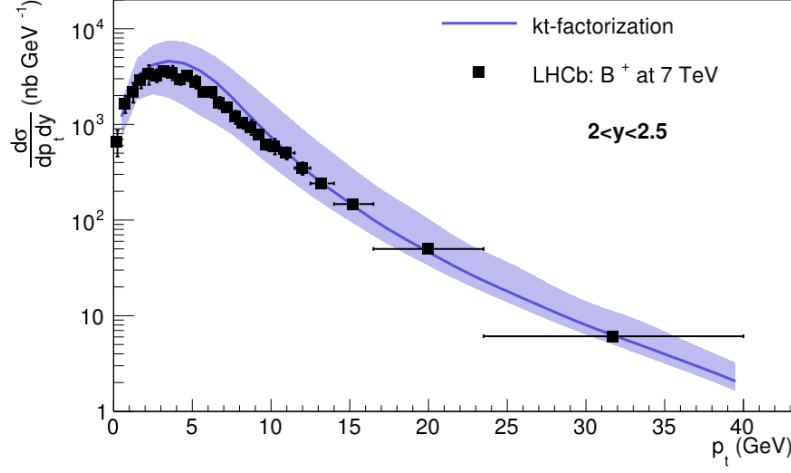


Figure 9: $(B^+ + B^-)$ production at 7 TeV compared with LHCb data [32].

bottom uPDF with μ , and to the fact that the main contribution is given by the flavor excitation process $gb \rightarrow gb$. Changing the Peterson for the Kartvelishvili et al. fragmentation function [33]

$$D(z) = (\alpha + 1)(\alpha + 2)z^\alpha(1 - z), \quad (16)$$

with $\alpha = 7$ gives a similar result. Our calculations at 13 TeV, presented in figure 10, show a similar agreement with LHCb data.

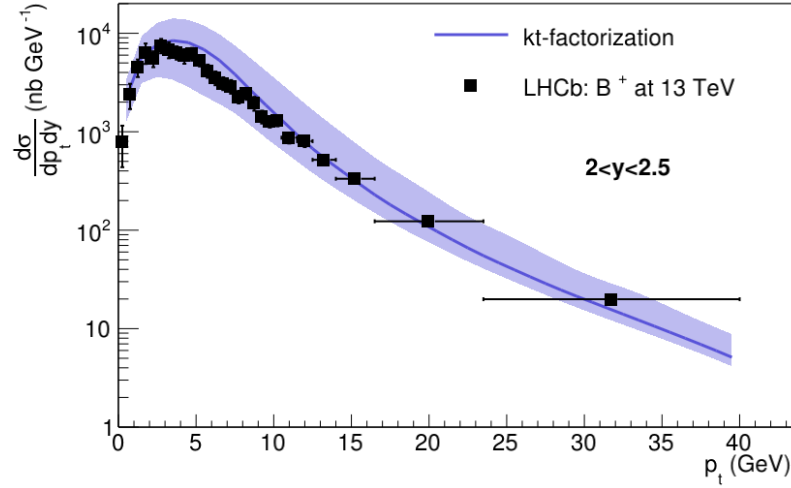


Figure 10: $(B^+ + B^-)$ production at 13 TeV compared with LHCb data [32].

5.3 B -meson production at very large rapidity

Keeping the same fragmentation function, we observe a deviation between our calculations and LHCb data in the rapidity range $4 < y < 4.5$, see Fig. 11. Changing parameter ϵ_b of the fragmentation function restores the agree-

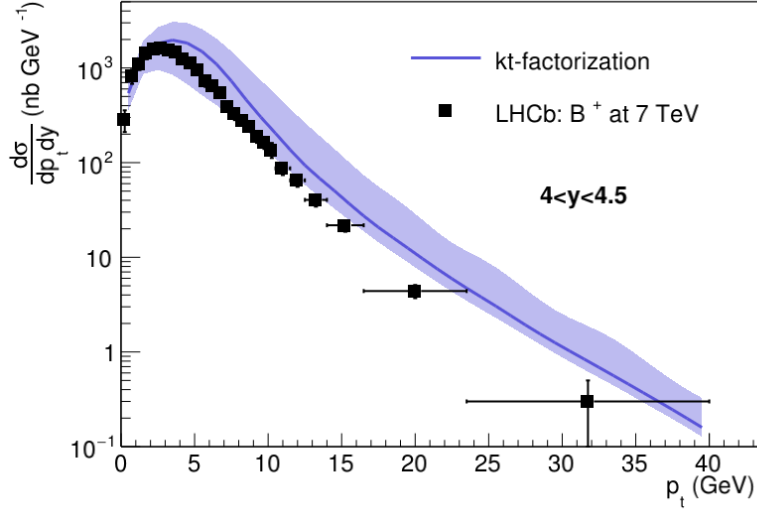


Figure 11: $(B^+ + B^-)$ production at 7 TeV compared with LHCb data [32] in the rapidity range $4 < y < 4.5$.

ment between theory and experiment. However, this change is unwanted as it implies a rapidity-dependent fragmentation function which is not part of the kt-factorization formalism, at least in its simplest formulation.

Our understanding of Fig. 11 is that it shows the limit of uPDFs built from collinear PDFs. Indeed, observables at large rapidities trigger smaller and larger values of x compared to central rapidity. From Figs. 1 and 2, we observe that the agreement between integrated uPDFs and collinear PDFs at $x = 0.01$ is not as good as at $x = 0.001$, and the situation is even worse at larger x . The agreement between integrated uPDFs (built from collinear PDFs) and collinear PDFs will never be perfect because relation (3) holds only approximately, see [13] for more details. We expect that uPDFs extracted directly from data will give a better description, and it seems to be the case. In Fig 12, we show a comparison between LHCb data for B mesons and our calculations, with our uPDFs replaced by the PB uPDFs [14]. The latter are obtained in a GM-VFNS by fitting experimental data. Note that the use of the PB uPDFs, extracted at the NNLO, with our NLO off-shell cross section is not consistent. However, in a VFNS, the numerical impact of this inconsistency is small. With the PB uPDFs, the agreement between

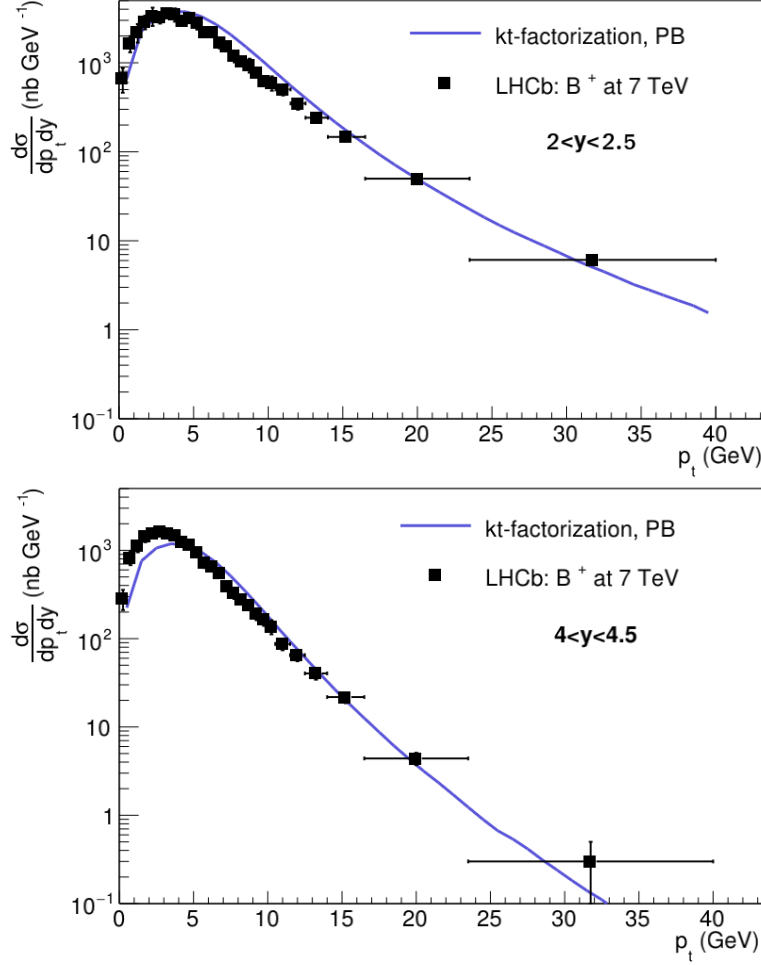


Figure 12: Results obtained with the PB uPDFs [14]. The LHCb data [32] are described satisfactorily in both rapidity ranges $2 < y < 2.5$ and $4 < y < 4.5$.

theory and experiment is good, including in the rapidity range $4 < y < 4.5$.

6 Treatment of the $2 \rightarrow 1$ process

It is sometimes believed that there is a double counting if we take into account both the $gg \rightarrow Q\bar{Q}$ and $gQ \rightarrow gQ$ processes. It is not the case since double counting happens between two different orders, for instance, when one adds the NLO contribution to a LO calculation. There is consequently no double counting between two LO or NLO processes. On the opposite, the leading-order contribution in k_t -factorization is given by the $2 \rightarrow 1$ process, and we can expect double counting between this process and the $2 \rightarrow 2$

processes used in this work. The goal of this section is to discuss this in more detail.

It is interesting to note that the LO and NLO graphs for deep inelastic scattering are similar to the $2 \rightarrow 1$ and $2 \rightarrow 2$ processes in k_t -factorization. At leading order, the virtual photon scatters from a (heavy) quark producing an on-shell quark⁴. At next-to-leading order, we find $2 \rightarrow 2$ processes such as $\gamma^* + g \rightarrow Q + \bar{Q}$. As explained in [19], there is a double counting between the LO and NLO contributions, because the production of the second particle in the NLO process is also accounted for by the evolution equation of the LO process. A subtraction term is required and the cross section reads

$$\sigma = \sigma^{\text{LO}} + \sigma^{\text{NLO}} - \text{subtraction term.} \quad (17)$$

In principle, finding the subtraction term is automatic. One should apply first collinear factorization at the partonic level, allowing to determine $\hat{\sigma}$, where the hat means that this partonic cross section is free of infrared divergences. In DIS at order α_s , the partonic cross section for heavy-quark production with the process initiated by the parton of flavor a is

$$\sigma_a^{(1)} = \sum_b (f_a^{b(0)} \otimes \hat{\sigma}_b^{(1)} + f_a^{b(1)} \otimes \hat{\sigma}_b^{(0)}), \quad (18)$$

where (0) and (1) refers to factors proportional to α_s^0 and α_s^1 , respectively. The functions $f_a^{b(n)}$ can be computed perturbatively, and correspond to the distribution of the parton b inside the parton a . The cross section $\hat{\sigma}_b^{(n)}$ is associated to the partonic process $\gamma^* + b \rightarrow Q + X$. Ref. [19] gives an explicit example for $a = g$. Using the fact that $\hat{\sigma}_a^{(0)} = \hat{\sigma}_a^{(0)}$ and $f_a^{b(0)}(\xi) = \delta_a^b \delta(1 - \xi)$ we have

$$\hat{\sigma}_a^{(1)} = \sigma_a^{(1)} - \sum_b f_a^{b(1)} \otimes \hat{\sigma}_b^{(0)} = \sigma_a^{(1)} - f_a^{Q(1)} \otimes \hat{\sigma}_Q^{(0)}, \quad (19)$$

where we replaced b by Q in the last equality, the LO process being $\gamma^* + Q \rightarrow Q$. This procedure automatically generates a term with a minus sign; the subtraction term. $\hat{\sigma}_a^{(1)}$ is free of infrared divergences due to the cancellation between $\sigma_a^{(1)}$ and $f_a^{b(1)}$. In a second step, factorization is applied at the hadronic level

$$\begin{aligned} \sigma &= f_{b/h} \otimes \hat{\sigma}_b \\ &= f_{Q/h} \otimes \sigma_Q^{(0)} + \sum_a \left(f_{a/h} \otimes \sigma_a^{(1)} - f_{a/h} \otimes f_a^{Q(1)} \otimes \hat{\sigma}_Q^{(0)} \right) \end{aligned} \quad (20)$$

where $f_{a/h}$ gives the distribution of a parton of flavor a in the hadron h . We believe that the fully consistent treatment of heavy-quark production

⁴The two differences with the $2 \rightarrow 1$ process in k_t -factorization is that the photon should be replaced by a gluon and the initial quark can be off-shell.

in k_t -factorization is given by Eq. (17), and we plan to work on this soon. However, it is possible to understand why the $2 \rightarrow 2$ process alone provides a good description of the experimental data. On the one hand, in DIS, there is a cancelation between the subtraction term and the LO term in the region $\mu > m_Q$ and $\alpha_s \ln(\mu/m_Q) \sim \mathcal{O}(1)$. It is the region studied in this work, and we expect a similar situation in k_t -factorization. On the other hand, we can argue that the $2 \rightarrow 1$ process at NLO, with a loop in the conjugate amplitude, is negligible with respect to the $2 \rightarrow 2$ process. Indeed, both contributions are of order $\mathcal{O}(\alpha_s^2)$, but the latter is enhanced by the divergences discussed in Sec. 4. Consequently, we can expect that the full contribution, Eq. (17), will be numerically close to the result given by the $2 \rightarrow 2$ process alone.

7 Conclusion

We have presented for the first time k_t -factorization calculations for heavy-quark production, using a GM-VFN scheme. We use uPDFs and off-shell cross section defined in this scheme at the order $\mathcal{O}(\alpha_s^2)$, sometimes misleadingly called leading order. Indeed, the leading order corresponds to the $2 \rightarrow 1$ process, and Eq. (17) shows how the LO and NLO contributions should be put together. We expect a nearly complete cancelation between the LO contribution and the subtraction term at moderate p_t , as well as a negligible role of the $2 \rightarrow 1$ process at one loop, justifying the use of the $2 \rightarrow 2$ contributions alone. However, the implementation of Eq. (17) could be important in the region $\mu \gg m_Q$, with potential application to jet physics.

The agreement between our calculations and experimental data is excellent, for both D and B mesons. In particular, the agreement has been improved compared to older k_t -factorization calculations, performed either in an FFN scheme or in a mix of VFN and FFN schemes. However, we have seen that at very large rapidity, our calculations fail if we use uPDFs built from collinear PDFs. In conclusion, accurate and consistent k_t -factorization calculations should be performed following the example of collinear factorization: the uPDFs should be extracted from data, and the cross section computed in a scheme identical to the one used for the uPDFs.

Acknowledgments

BG acknowledges support from Chilean FONDECYT Iniciación grant 11181126. BG is supported by ANID PIA/APOYO AFB180002 (Chile). AvH is supported by grant no. 2019/35/B/ST2/03531 of the Polish National Science Centre.

References

- [1] M. Cacciari, Rise and Fall of the Bottom Quark Production Excess, [arXiv:hep-ph/0407187 \(2004\)](#).
- [2] S. Catani, M. Ciafaloni and F. Hautmann, Gluon contributions to small x heavy flavour production, [Phys. Lett. B 242 \(1990\) 97-102](#).
- [3] J.C. Collins and R.K. Ellis, Heavy-quark production in very high energy hadron collision, [Nucl. Phys. B 360 \(1991\) 3-30](#).
- [4] S. Catani, M. Ciafaloni and F. Hautmann, High energy factorization and small- x heavy flavour production, [Nucl. Phys. B 366\(1991\) 135-188](#).
- [5] E. M. Levin, M. G. Ryskin, Y. M. Shabelski, A. G. Shuvaev, Heavy quark production in semihard nucleon interaction, *Sov. J. Nucl. Phys.* 53 (1991) 657.
- [6] A. V. Lipatov, V. A. Saleev, and N. P. Zotov, Heavy Quark Production at the TEVATRON in the Semihard QCD Approach and the Unintegrated Gluon Distribution, [arXiv:hep-ph/0112114v3 \(2001\)](#).
- [7] H. Jung, Heavy quark production at the TEVATRON and HERA using k_t factorization with CCFM evolution, [Phys. Rev. D 65 \(2002\) 034015](#).
- [8] H. Jung, M. Kraemer, A.V. Lipatov, and N.P. Zotov, Heavy Flavour Production at Tevatron and Parton Shower Effects, [JHEP 01 \(2011\) 085](#).
- [9] R. Maciula, A. Szczurek, Open charm production at the LHC - k_t -factorization approach, [Phys. Rev. D 87 \(2013\) 094022](#).
- [10] Yu. M. Shabelski, A. G. Shuvaev, and I. V. Surnin, Heavy quark production in kt factorization approach at LHC energies, [Int. J. Mod. Phys. A33, 1850003 \(2018\)](#).
- [11] R. Maciula, A. Szczurek, Consistent treatment of charm production in higher-orders at tree-level within k_t -factorization approach, [Phys.Rev.D 100 \(2019\) 5, 054001](#).
- [12] B. Guiot, Heavy-quark production with k_t -factorization: The importance of the sea-quark distribution, [Phys.Rev.D 99 \(2019\) 7, 074006](#).
- [13] B. Guiot, Pathologies of the Kimber-Martin-Ryskin prescriptions for unintegrated PDFs: Which prescription should be preferred?, [Phys.Rev.D 101 \(2020\) 5, 054006](#).

- [14] A. B. Martinez, P. Connor, F. Hautmann, H. Jung, A. Lelek, V. Radescu, and R. Zlebcik, Collinear and TMD parton densities from fits to precision DIS measurements in the parton branching method, [Phys.Rev.D 99 \(2019\) 7, 074008](#).
- [15] F. Hautmann, H. Jung, M. Krämer, P. J. Mulders, E. R. Nocera, T. C. Rogers and A. Signori, TMDlib and TMDplotter: library and plotting tools for transverse-momentum-dependent parton distributions, [Eur. Phys. J. C 74 \(2014\) 3220](#).
- [16] N. A. Abdulov *et al.*, TMDlib2 and TMDplotter: a platform for 3D hadron structure studies, [arXiv:2103.09741](#).
- [17] G. Watt, A.D. Martin and M.G. Ryskin, Unintegrated parton distributions and inclusive jet production at HERA, [Eur. Phys. J. C 31\(2003\) 73](#).
- [18] S. Dulat *et. al.*, New parton distribution functions from a global analysis of quantum chromodynamics, [Phys. Rev. D 93 \(2016\) no.3, 033006](#).
- [19] M. A. G. Aivazis, J. C. Collins, F. I. Olness and W.-K. Tung, Lepton production of heavy quarks. II. A unified QCD formulation of charged and neutral current processes from fixed-target to collider energies, [Phys. Rev. D 50, 3102 \(1994\)](#).
- [20] J. C. Collins, Hard-scattering factorization with heavy quarks: A general treatment, [Phys. Rev. D 58, 094002 \(1998\)](#).
- [21] W.-K. Tung, S. Kretzer and C. Schmidt, Open heavy flavour production: conceptual framework and implementation issues, *J. Phys. G* 28, 983 (2002) [[hep-ph/0110247](#)].
- [22] A. van Hameren, KaTie : For parton-level event generation with k_T -dependent initial states, [Comput. Phys. Commun. 224 \(2018\), 371-380](#).
- [23] J. Alwall, *et al.*, A Standard format for Les Houches event files, [Comput. Phys. Commun. 176 \(2007\), 300-304](#).
- [24] A. van Hameren, P. Kotko and K. Kutak, Helicity amplitudes for high-energy scattering, [JHEP 01 \(2013\), 078](#).
- [25] A. van Hameren, K. Kutak and T. Salwa, Scattering amplitudes with off-shell quarks, [Phys. Lett. B 727 \(2013\), 226-233](#).
- [26] C. Peterson, D. Schlatter, I. Schmitt, P.M. Zerwas, Scaling violations in inclusive e^+e^- annihilation spectra, [Phys. Rev. D 27 \(1983\) 105](#).

- [27] M. Cacciari, M. Greco and P. Nason, “The $p(T)$ spectrum in heavy-flavor hadroproduction”, [JHEP 05 \(1998\) 007](#);
M. Cacciari, S. Frixione and P. Nason, “The $p(T)$ spectrum in heavy-flavor photoproduction”, [JHEP 03 \(2001\) 006](#).
- [28] S. Acharya et al., Measurement of D-meson production at mid-rapidity in pp collisions at $\sqrt{s} = 7$ TeV, [Eur.Phys.J.C 77 \(2017\) 8, 550](#).
- [29] S. Acharya et al., Measurement of beauty and charm production in pp collisions at $\sqrt{s} = 5$ TeV, via non-prompt and prompt D mesons, [JHEP 05 \(2021\) 220](#).
- [30] LHCb Collaboration, Roel Aaij et al., Measurements of prompt charm production cross-sections in pp collisions at $\sqrt{s} = 13$ TeV, [JHEP 03 \(2016\) 159](#), [JHEP 09 \(2016\) 013](#) (erratum), [JHEP 05 \(2017\) 074](#) (erratum)
- [31] M. Cacciari et al., Theoretical predictions for charm and bottom production at the LHC, [JHEP 10 \(2012\) 137](#).
- [32] R. Aaij et al., Measurement of the B^\pm production cross-section in pp collisions at $\sqrt{s} = 7$ and 13 TeV, [JHEP 12 \(2017\) 026](#).
- [33] V. G. Kartvelishvili, A. K. Likhoded, V. A. Petrov, [Phys.Lett.B 78 \(1978\) 615-617](#).

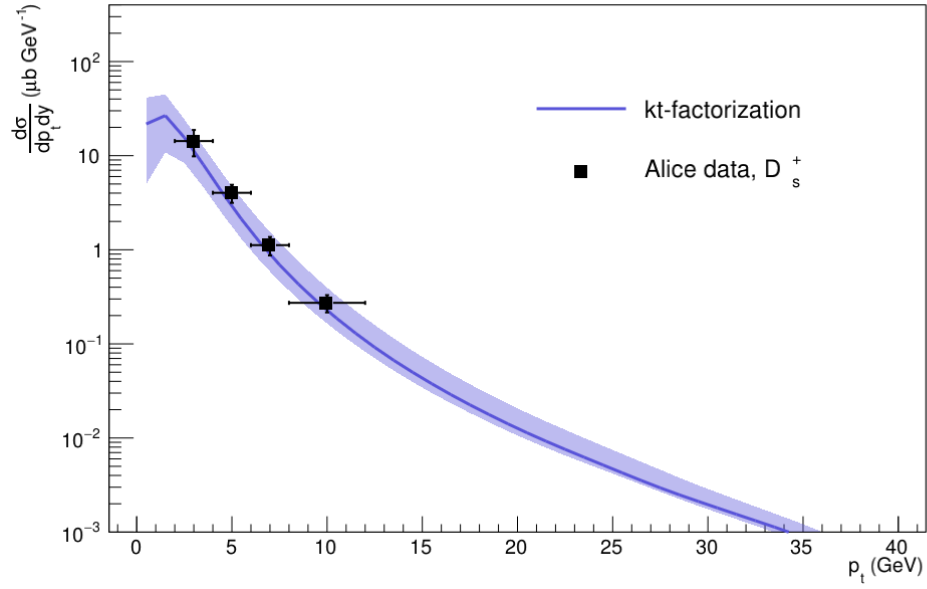
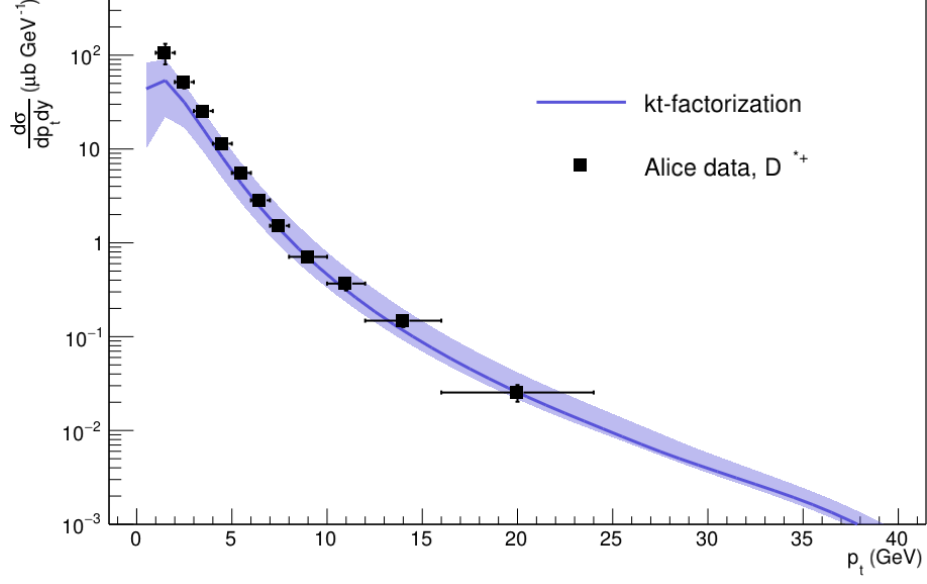


Figure 13: Results for D^{*+} and D_s^+ mesons compared to ALICE data at 7 TeV [28].